Journal of Catalysis 268 (2009) 307–317

Contents lists available at ScienceDirect

Journal of Catalysis

journal homepage: www.elsevier.com/locate/jcat

Influence of textural properties and trace water on the reactivity and deactivation of reconstructed layered hydroxide catalysts for transesterification of tributyrin with methanol

Yuanzhou Xi, Robert J. Davis *

Department of Chemical Engineering, University of Virginia, 102 Engineers' Way, P.O. Box 400741, Charlottesville, VA 22904-4741, USA

ARTICLE INFO

Article history:
Received 7 August 2009
Revised 28 September 2009
Accepted 30 September 2009
Available online 31 October 2009

Keywords:
Biodiesel
Reconstruction
Brønsted base site
Lewis base site
Phenol adsorption
Intercalation

ABSTRACT

Magnesium–aluminum hydrotalcites with a Mg/Al molar ratio of 2 were prepared by coprecipitation or by urea hydrolysis. The as-prepared samples, as well as their activated analogues, were characterized by N_2 physisorption, phenol chemisorption, SEM, XRD, TGA, and DRIFTS. The base-catalyzed transesterification of tributyrin with methanol at 333 K was used to probe the reactivity of the materials. The reconstructed hydrotalcite samples exhibited much higher catalytic activity than the mixed oxides of Mg and Al. Nevertheless, the turnover frequency for the reaction was about two orders of magnitude lower than that of homogeneous sodium methoxide. Variations in the textural properties of the reconstructed hydrotalcite catalysts did not significantly affect the surface base site density or the turnover rate of transesterification. However, the presence of trace water not only enhanced the transesterification reaction rate but also led to severe catalyst deactivation. Characterization of deactivated catalysts revealed a replacement of the interlayer Brønsted base sites with butyric anions, which led to an expansion of the interlayer distance.

1. Introduction

Solid base catalysts are potentially useful for a wide variety of organic chemical syntheses such as double bond isomerization, hydrogenation, amination, aldol condensation, and Michael addition. Because solid bases are easily separated from the reaction media, they are attractive alternatives to traditional homogeneous base catalysts that cause serious environmental problems and require complicated downstream separation and neutralization processes [1–4].

Hydrotalcite is a layered double hydroxide with the general formula $[Mg_{(1-x)}Al_x(OH)_2]^{x+}(CO_3^{2-})_{x/2}\cdot nH_2O$. It is a well-studied solid base precursor that belongs to a class of anionic clays having positively charged brucite-like layers and carbonate anions residing in the interlayer regions together with some water molecules. The decomposition of hydrotalcite generates a high surface area Mg–Al mixed oxide that exposes a variety of base sites on the solid surface. The basic properties of the mixed oxide depend on the Mg–Al ratio in the hydrotalcite precursor and on the preparation method [2,5,6]. The mixed oxide catalyst is known to catalyze aldol condensation [7], alkylation [8], and double-bond isomerization [9]. Reconstruction of the layered hydrotalcite from a decomposed sample by exposure to water generates Brønsted base sites between the new layers. These reconstructed layered materials demonstrate higher catalytic activity than the Mg–Al mixed oxides in a variety of reactions such as aldol condensation of citral with ketones [10], acetone self-condensation [11,12], Michael addition [13], transesterification of tributyrin with methanol [14,15] and styrene epoxidation [16]. Previous studies suggest that the active sites reside mainly near the edges of hydrotalcite platelets [10–12,17–19]. Furthermore, Chimentao et al. [16] proposed that defects in the lamellar structure of hydrotalcite nanoplatelets increase the accessibility of the base sites. However, Roeffaers et al. [20] observed that the transesterification of 5-carboxyfluorescein with 1-butanol over $[Li^+–Al^{3+}]$-layered double hydroxide catalyst occurs on the basal planes of the outer crystal surface without preference for the crystal edges, whereas the hydrolysis reaction takes place on the crystal edges. In addition, Greenwell et al. [21] and Lei et al. [22] found that activated hydrotalcite with higher crystallinity prepared via urea hydrolysis shows much higher catalytic activity for aldol condensation, suggesting that the ordered surface hydroxyl groups or enhanced lamellar structure might also be important for catalysis.

Unfortunately, the highly active reconstructed hydrotalcite catalysts often deactivate rapidly. For example, Winter et al. [18] reported that a recycled carbon nanofiber-supported hydrotalcite without regeneration shows less than 1/7 of the original activity for acetone self-condensation, although a tedious reactivation via heat treatment and rehydration can regenerate about 90% of the

* Corresponding author. Fax: +1 434 982 2658.
E-mail addresses: yx8f@virginia.edu (Y. Xi), rjd4f@virginia.edu (R.J. Davis).

0021-9517/$ - see front matter © 2009 Elsevier Inc. All rights reserved.
doi:10.1016/j.jcat.2009.09.029

original activity. More recently, Abello et al. [23] studied the air stability, reusability, and regenerability of activated hydrotalcite for aldol condensations. They found that activated hydrotalcite exposed to air for 1 h loses 50% of its activity. Moreover, a recycled catalyst is almost inactive and a time-consuming reactivation procedure is needed for the regeneration of the active sites. A recent study from our laboratory on the use of activated hydrotalcite for transesterification of tributyrin with methanol, a model reaction of biodiesel production [14], showed that a reconstructed hydrotalcite deactivates faster than the mixed oxide, although the former is initially one order of magnitude more active than the latter [15]. In addition, the reconstructed hydrotalcite experiences severe activity loss upon thermal treatment at the relatively mild temperature of 473 K [15]. Liu et al. [24] and Lopez et al. [24,25] studied solid base catalysts for biodiesel production, and deactivation was also observed.

In this work, the catalytic activity and stability of hydrotalcites with various textural properties were studied in the transesterification of tributyrin with methanol. The influence of trace water on the reaction was also investigated. The hydrotalcites were prepared by two different synthesis methods (coprecipitation or urea hydrolysis) and were reconstructed using two different water treatments (liquid-phase hydrothermal treatment or gas-phase treatment).

2. Experimental methods

2.1. Catalyst synthesis

A constant pH coprecipitation method was used to prepare Mg–Al hydrotalcite with a Mg/Al molar ratio of 2. A 300 ml of an aqueous solution containing 76.91 g (0.3 mol) of $Mg(NO_3)_2{\cdot}6H_2O$ (Acros, 98%) and 56.25 g (0.15 mol) of $Al(NO_3)_3{\cdot}9H_2O$ (Aldrich, 98%), and another 300 ml of aqueous solution containing 15.90 g (0.15 mol) of Na_2CO_3 (Aldrich, 99.95%) were added dropwise into 80 ml of distilled deionized (DDI) water vigorously stirred at 333 K for about 30 min. The pH of the mixture was maintained at 10 by adding dropwise a 4 mol L^{-1} solution of NaOH (Mallinckrodt, 99%). After the slurry was stirred for 24 h at 333 K, the white precipitate was recovered by centrifugation and washed thoroughly with DDI water. The precipitate was then dried in air in an oven at 338 K for 24 h and ground into a powder and sieved between 0.038 and 0.075 mm. The resulting catalyst precursor is denoted as CHT for "coprecipitated hydrotalcite".

A hydrothermal method involving urea hydrolysis [26] was also used to synthesize Mg–Al hydrotalcite with a Mg/Al molar ratio of 2 [22]. A 500 ml of an aqueous solution containing 25.64 g (0.1 mol) of $Mg(NO_3)_2{\cdot}6H_2O$, 18.76 g (0.05 mol) of $Al(NO_3)_3{\cdot}9H_2O$, and 84.08 g (1.4 mol) of urea (Fluka, 99.5%) was sealed in Teflon vessels and heated to 363 K for 3 days. The crystallized hydrotalcite was then centrifuged, washed, dried, and sieved according to the same procedure as used for CHT. The Mg–Al hydrotalcite prepared by urea hydrolysis is denoted as UHT for "urea hydrotalcite".

2.2. Catalyst activation

The synthetic Mg–Al hydrotalcites were activated by either thermal decomposition or thermal decomposition followed by reconstruction. The decomposed Mg–Al hydrotalcites, denoted as CHT-d or UHT-d, were prepared by heating 1 g of fresh sample under flowing dry N_2 (100 cm^3 min^{-1}) (Messer, 99.999%) at 723 K (after heating at a rate of 10 K min^{-1}) for 8 h. The decomposed hydrotalcites were reconstructed by hydrothermal treatment by dispersing the decomposed 1 g of Mg–Al hydrotalcite into 100 ml of decarbonated DDI water and heating the slurry in a sealed Teflon vessel at 413 K for 24 h. After cooling to room temperature, the solid catalyst was separated by centrifugation and washed with 200 ml of methanol (Fisher, 99.9%). The samples reconstructed by hydrothermal treatment are denoted as CHT-d-rl or UHT-d-rl. Before characterization of the reconstructed samples, they were dried in flowing N_2 (100 cm^3 min^{-1}) overnight at room temperature. In addition, vapor-phase water was also used to reconstruct CHT-d. In summary, flowing wet N_2 (2.6 vol% gas-phase water, by bubbling N_2 at 100 cm^3 min^{-1} through 200 ml of 9.1% NaCl aqueous solution) was passed through a bed of decomposed CHT sample for 24 h at room temperature. The sample denoted as CHT-d-rg was then washed with 200 ml of methanol prior to catalysis to be consistent with the pretreatment of samples prepared by hydrothermal reconstruction.

One reconstructed hydrotalcite was intentionally intercalated with butyric anion. The reconstructed sample, CHT-d-rl, was first prepared from 1 g of CHT. After thermal decomposition and hydrothermal reconstruction were complete at 413 K, the cooled sample in liquid water was transferred to a 3-necked round-bottomed flask. Next, 920 μL of butyric acid (Aldrich, 99%) was added to the catalyst slurry. After stirring the mixture at 800 rpm for 24 h at room temperature, the solid was again separated by centrifugation, washed with 200 ml of methanol, and dried under flowing N_2 (100 cm^3 min^{-1}) before characterization.

2.3. Catalyst characterization

The composition of the hydrotalcite samples (Mg/Al molar ratio and Na content) was measured by ICP analysis (Galbraith Laboratories, Knoxville, TN). Physisorption of N_2 was performed at 77 K using a Micromeritics ASAP 2020 after the samples were degassed for 2 h at 298 K. The surface area and pore size distribution were calculated by the Brunauer–Emmett–Teller (BET) method and Barrett–Joyner–Hallender (BJH) method, respectively. The X-ray diffraction patterns were recorded on a Scintag XDS 2000 diffractometer using Cu Kα radiation (λ = 1.54 Å). The samples were scanned continuously from 4° to 72° at a scan rate of 2° min^{-1}. Scanning electron microscopy (SEM) of the samples coated with Au–Pd was measured on a JEOL-6700F field emission microscope.

The diffuse reflectance infrared Fourier transformed spectra (DRIFTS) were recorded on a BIO-RAD FTS-60A spectrometer equipped with a Harrick Praying Mantis diffuse reflectance accessory purged with flowing N_2. The spectra were averaged from 100 scans recorded at a resolution of 4 cm^{-1} in the range of 400–4000 cm^{-1}. During sample preparation, the catalysts were briefly exposed to ambient atmosphere and diluted in KBr powder at 5 wt%. Pure KBr powder was used as the background.

Thermogravimetric analysis (TGA) was performed on a TGA 2050 Thermogravimetric analyzer (TA Instruments). Approximately 40 mg of hydrotalcite sample was used and the temperature was ramped from room temperature to 723 K at 2 K min^{-1} under 100 cm^3 min^{-1} of flowing N_2.

The density of base sites of the reconstructed hydrotalcite samples was determined by phenol adsorption. Before measurement, methanol-washed reconstructed hydrotalcite samples were dried under flowing N_2 (100 cm^3 min^{-1}) overnight at room temperature. The dried catalysts were weighed (50 mg) under N_2 atmosphere and added to 25 ml solutions of phenol (Aldrich, 99.5%) in cyclohexane (Aldrich, 99.5%) in stoppered bottles filled with N_2. The mixtures were then shaken for 3 h at room temperature. The concentration of phenol in the cyclohexane solvent after adsorption was evaluated by a Cary 3E UV spectrometer (λ_{max} = 271 nm) after filtering the mixture with 0.2 μm PTFE syringe filter. The phenol adsorption isotherms on reconstructed hydrotalcite samples obeyed the Langmuir adsorption equation: $X/X_m = KC/(1 + KC)$,

where C is the equilibrium concentration of phenol (mmol L^{-1}), K is a constant (mmol L^{-1}), X is the amount of adsorbed phenol per surface area of catalyst (mmol m^{-2}), and X_m is the monolayer phenol coverage (mmol m^{-2}), which corresponds to the density of the base sites of reconstructed hydrotalcite samples.

2.4. Transesterification catalysis

The catalytic transesterification reactions were conducted in a 250 ml 3-necked round-bottomed flask at 333 K in an oil bath and magnetically stirred at 800 rpm. The reactor was equipped with a reflux condenser and was continuously purged with flowing N_2 at 40 cm^3 min^{-1}. Unless otherwise indicated, methanol (Fisher, 99.9%) and tributyrin (Aldrich, 99%) were used as reactants. In each run, 68.25 g of methanol and 21.9 g of tributyrin were charged into the reactor with 3.3 g of dibutyl ether (Aldrich, 99.3%) as an internal standard. After the temperature of the reactants reached 333 K, the activated catalyst from 1 g UHT or CHT was added to the reactor to initiate transesterification. During the catalyst pretreatments, care was taken to prevent CO_2 contamination. The decomposed hydrotalcite catalysts and the gas-phase reconstructed sample were directly transferred to the reactor to avoid CO_2 contamination from air. The hydrothermally reconstructed catalysts were kept either in DDI water or in methanol during any washing or transferring step without any exposure of the dry powder form to air to minimize CO_2 contamination. Liquid samples were removed from the reactor at different time intervals and analyzed for products using the same procedure described in the previous work [15].

Some reaction tests were conducted with purified tributyrin to fully exclude the deactivation due to the possible carboxylic acid impurities from tributyrin source. To obtain purified tributyrin, a mixture of 100 ml of tributyrin and 40 ml of saturated sodium carbonate aqueous solution (23.5 wt%) was vigorously stirred for 20 h at room temperature. Then the mixture was allowed to settle and the organic layer was separated. Approximately 16 g of 723 K activated 3A molecular sieves were added to the organic layer and the mixture was allowed to sit at room temperature overnight. After the tributyrin was separated from the molecular sieves, vacuum distillation was performed to obtain purified tributyrin. In some cases, anhydrous methanol (Aldrich, 99.8%) was used as the reactant.

To test the effect of catalyst recycling on activity, the used catalyst was separated from the product solution by centrifugation and washed with 200 ml of methanol prior to charging back into the reactor with fresh reactants. After the second reaction was conducted for about 20 h, the used catalyst was removed by centrifugation, washed with 200 ml of methanol, and dried under flowing dry N_2 (100 cm^3 min^{-1}) prior to characterization.

The transesterification of tributyrin (T) with methanol (M) proceeds in three consecutive steps as shown in the following reaction equations:

$$T + M \xrightarrow{k_1} D + MB, \quad (1)$$

$$D + M \xrightarrow{k_2} Mo + MB, \quad (2)$$

$$Mo + M \xrightarrow{k_3} G + MB, \quad (3)$$

where D, MB, Mo, and G denote dibutyrin, methyl butyrate, monobutyrin, and glycerol, respectively. The reaction was assumed to be essentially irreversible and pseudo first order because of the great excess of methanol. The pseudo first order kinetic model with respect to the butyrin components was used here to quantify the reaction rate constants on a surface area basis k_1, k_2, k_3 (mol^{-1} L m^{-2} min^{-1}), and the deactivation parameter α (min^{-1}) [15].

3. Results and discussion

3.1. Elemental analysis

The Mg/Al molar ratio of CHT and UHT was 1.98 and 1.75, respectively, as determined by ICP elemental analysis, which is close to the nominal ratio of 2. The trace amount of sodium in the CHT sample was measured at less than 0.07 wt%. Upon hydrothermal reconstruction of decomposed CHT and UHT samples, the Mg/Al molar ratio remained constant as shown in Table 1. Evidently, hydrothermal reconstruction did not preferentially remove any of the components.

3.2. Catalyst morphology

Scanning electron microscopy (SEM) was used to visualize the particle morphology of the hydrotalcite samples upon decomposition and reconstruction. The CHT and UHT samples exhibited significant differences in platelet sizes as revealed in Fig. 1. The hydrotalcite prepared by urea hydrolysis showed a well-developed layered structure with mono-dispersed platelets about 1.0–1.5 μm in the a–b plane and about 100 nm in thickness (c-axis) as illustrated in Fig. 1a. The hydrotalcite prepared by coprecipitation also showed a well-developed layered structure, but with much smaller platelets around 40–70 nm (in the a–b plane) as presented in Fig. 1A. These small platelets aggregate to form a porous particle. The overall morphology of the decomposed hydrotalcites UHT-d and CHT-d shown in Fig. 1b and Fig. 1B was similar to that of their corresponding precursors, which is consistent with the previously reported results [19,27]. However, the decomposed UHT platelets tended to experience partial exfoliation upon hydrothermal reconstruction as illustrated in Fig. 1c. The platelets appeared to grow in

Table 1
Physical and chemical properties of hydrotalcite samples.

Sample	Mg/Al molar ratio[a]	S_{BET} (m^2 g^{-1})	Pore volume (cm^3 g^{-1})	d_{003} (Å)	a (Å)	$D(0\,0\,l)$[b,c] (Å)	$D(1\,1\,0)$[b] (Å)	Base sites density[d] (mmol m^{-2})
UHT	1.75	14	0.04	7.39	3.03	332	231	–
UHT-d	–	258	0.19	–	–	–	–	–
UHT-d-rl	1.72	50	0.19	7.40	3.04	170	243	0.024 (24.5%)[e]
CHT	1.98	71	0.36	7.41	3.03	209	283	–
CHT-d	–	252	0.62	–	–	–	–	–
CHT-d-rl	1.95	67	0.31	7.41	3.04	169	275	0.020 (32.5%)[e]
CHT-d-rg	–	49	0.26	7.56	3.04	54	99	0.023 (22.8%)[e]

[a] ICP elemental analysis.
[b] The Debye–Scherrer equation [64] was used to estimate the average crystallite size. The full width at half maximum (FWHM) of the diffraction peaks was obtained by fitting the XRD patterns by using the pseudo-Voigt functions. Silicon was used as a standard to estimate the instrumental line broadening.
[c] The crystallite size along the normal of (0 0 l) was averaged from $D(0\,0\,3)$ and $D(0\,0\,6)$.
[d] The base sites density is the phenol monolayer coverage, X_m, as measured by phenol adsorption experiments.
[e] The number between parentheses represents the ratio of phenol uptake to total base sites, determined from Al content.

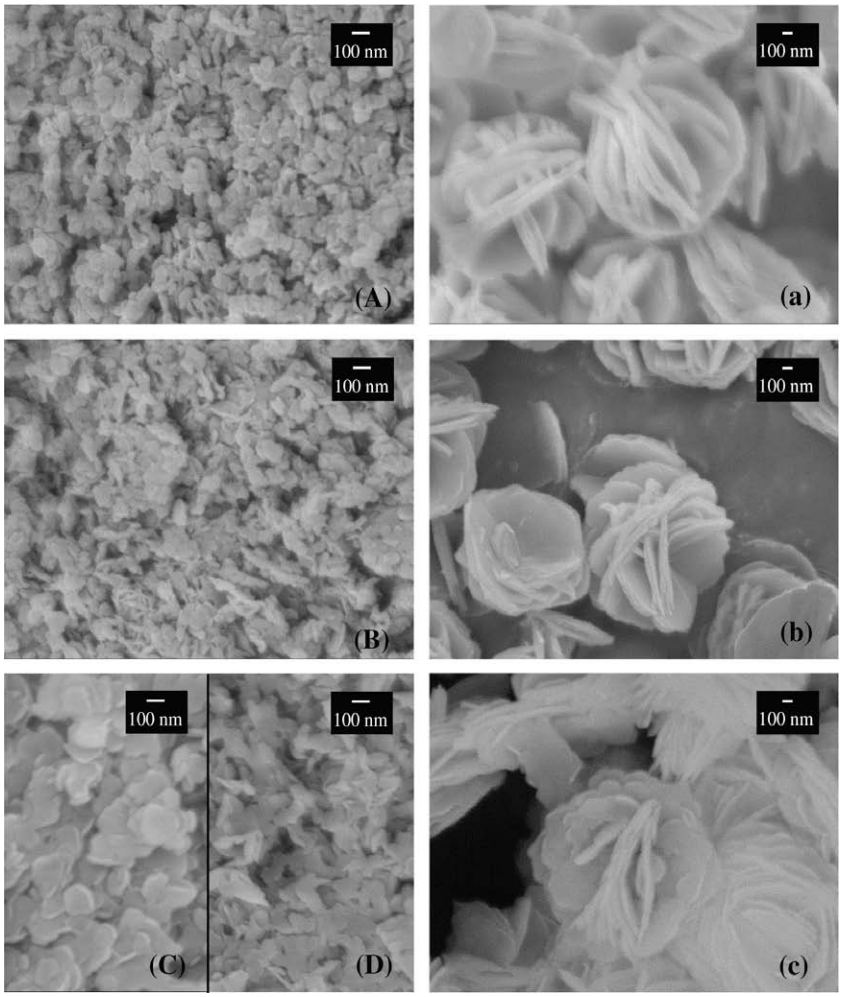

Fig. 1. Scanning electron micrographs of hydrotalcite samples. (A) CHT; (B) CHT-d; (C) CHT-d-rl; (D) CHT-d-rg; (a) UHT; (b) UHT-d; (c) UHT-d-rl.

the a–b plane to about 1.5–2.0 μm but formed thinner layers, around 50 nm. The hydrothermally reconstructed CHT sample experienced an apparent increase in platelet size as shown in Fig. 1C. The CHT-d-rl platelets grew significantly to 150–250 nm, presumably through a dissolution–reprecipitation mechanism [28]. The platelet size of CHT-d-rg slightly increased to 90–110 nm as shown in Fig. 1D.

3.3. Estimation of crystallite size

The X-ray diffraction (XRD) patterns of as-prepared and activated hydrotalcite samples from both coprecipitation and urea hydrolysis are presented in Fig. 2. Both CHT and UHT exhibited Mg–Al hydrotalcite reflections associated with the layered double hydroxide crystal structure. The (0 0 3) and (0 0 6) reflections at 11.9° and 23.8° can be used to calculate the basal spacing, *d*, between the layers. The (1 1 0) reflection at 61.1° can be used to calculate the unit cell parameter, *a*, where $a = 2d_{110}$ [5]. The calculated results are illustrated in Table 1. Hydrotalcite prepared by hydrothermal synthesis via urea hydrolysis has better developed crystals than a sample that was prepared by simple coprecipitation, as seen from the sharper and much more symmetric peaks at 35.3°, 39.9°, and 47.4°, corresponding to (0 1 2), (0 1 5), and (0 1 8) reflections, respectively, indicating less stacking disorder [29–32] and turbostratic disorder [29,31], which is consistent with the previously reported results [33]. Both UHT and CHT samples lose their hydrotalcite-layered structure after decomposition at 723 K for 8 h and form a porous mixed oxide of Mg and Al. Only the MgO structure can be detected by XRD as shown in Fig. 2c and d. The layered structures of the decomposed hydrotalcite samples were successfully reconstructed by hydrothermal treatment in liquid water at 413 K for 24 h or, for one case, by gas-phase reconstruction involving passing wet N_2 through a decomposed hydrotalcite sample bed for 24 h [5,34]. Interestingly, the reconstructed hydrotalcite CHT-d-rl had stronger peak intensities from the layers than those of UHT-d-rl. The UHT-d-rl sample had much broader (0 *k l*) peaks (30–50°) than its precursor, indicating that stacking and/or turbostratic disorder developed during the reconstruction process. The gas-phase reconstructed sample CHT-d-rg showed a very weak diffraction pattern; nevertheless, the disappearance of the MgO phase suggests that the layered structure was reconstructed. The basal spacing, *d*, and unit cell parameter, *a*, of the CHT and UHT samples and their hydrothermally reconstructed analogues were almost identical at 7.40 Å and 3.03 Å, respectively, as shown in Table 1. It should be noted that UHT-d could not be reconstructed with gas-phase water. Hydrothermal reconstruction was required in that case.

The line broadening from XRD patterns of hydrotalcite samples has been used to estimate the crystallite size according to the Debye–Scherrer equation [18,35–37]. The XRD line broadening of (0 0 3), (0 0 6), and (1 1 0) reflections of the layered materials was used to estimate the crystallite size in this work, since they are less affected by stacking disorder and turbostratic disorder [29]. The results are summarized in Table 1. The UHT sample had

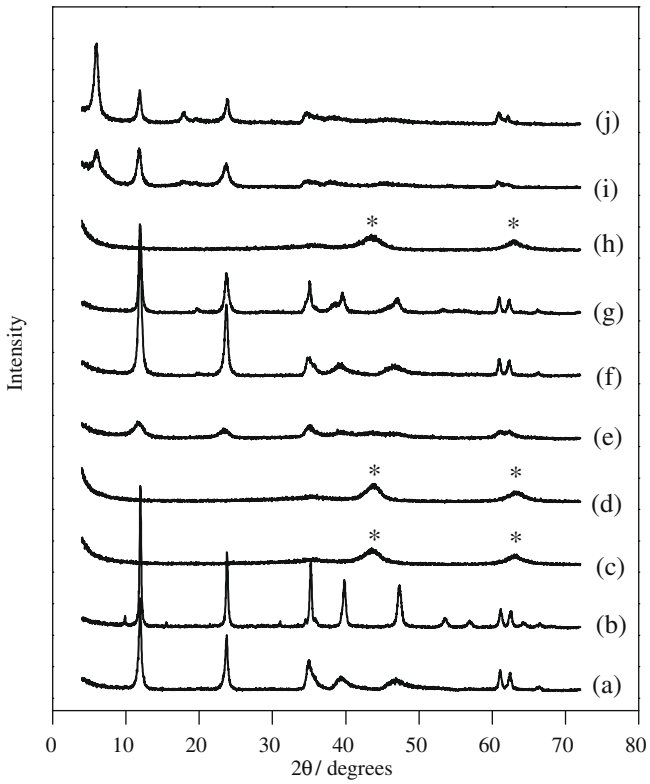

Fig. 2. X-ray diffraction patterns of (a) CHT; (b) UHT; (c) CHT-d; (d) UHT-d; (e) CHT-d-rg; (f) CHT-d-rl; (g) UHT-d-rl; (h) recycled CHT-d after 2 runs; (i) recycled CHT-d-rl after 2 runs (purified tributyrin and anhydrous methanol were used as reactants); and (j) butyric acid-treated CHT-d-rl. * Represents features found in MgO.

a much larger crystallite size than the CHT sample along the normal of (0 0 *l*) whereas the opposite was found along the normal of (1 1 0). The crystallite size of the reconstructed samples was generally smaller than that of their corresponding precursor, with the exception of UHT-d-rl along the normal of (1 1 0). More importantly, the crystallite size of the gas-phase reconstructed sample (CHT-d-rg) was significantly smaller than that of either of the hydrothermally reconstructed samples.

3.4. Thermogravimetric analysis

The results from thermogravimetric analysis (TGA) of the fresh hydrotalcite samples, UHT and CHT, and their reconstructed samples are shown in Fig. 3. All the fresh hydrotalcite samples and their reconstructed analogues display two weight loss steps during the thermal decomposition process [38,39]. The first weight loss that occurred below 490 K is ascribed to the removal of physisorbed and interlayer water. The second weight loss above 490 K is attributed to dehydroxylation of the brucite-like layers and decarbonation of as-prepared hydrotalcite or dehydroxylation of the interlayer Brønsted hydroxyl anions of reconstructed hydrotalcite.

3.5. Adsorption of N_2

Adsorption of N_2 was used to measure the surface area and pore size distribution of the hydrotalcites and their activated forms and the results are summarized in Table 1 and Fig. 4. The as-prepared UHT sample revealed low porosity (0.04 $cm^3\ g^{-1}$ pore volume) and low surface area (14 $m^2\ g^{-1}$). Upon thermal decomposition, the pore size distribution between 10 and 100 nm only slightly increased, whereas small pores less than 3 nm apparently formed as

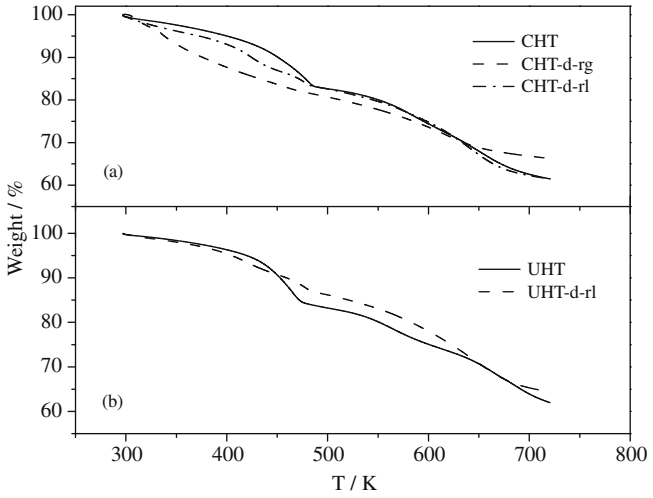

Fig. 3. Thermogravimetric analysis (TGA) of (a) CHT and reconstructed CHT samples and (b) UHT and reconstructed UHT samples.

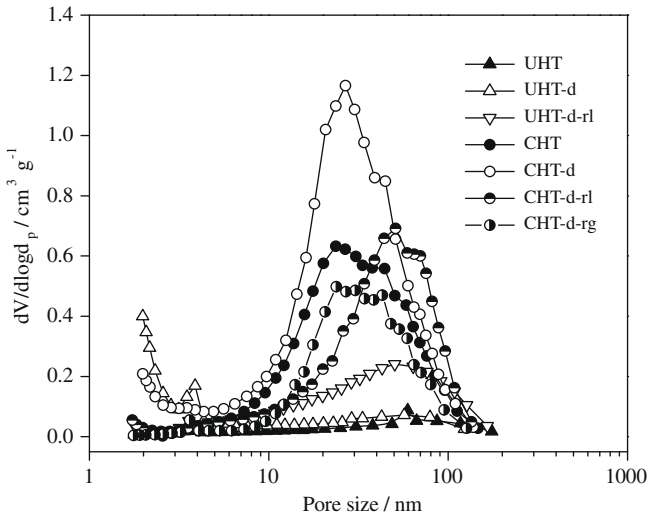

Fig. 4. Pore size distribution of CHT and UHT and their derived catalysts calculated from N_2 desorption branch using BJH method.

shown in Fig. 4, resulting in a total pore volume increase to 0.19 $cm^3\ g^{-1}$. The BET surface area of UHT-d increased significantly to 258 $m^2\ g^{-1}$, mainly due to the creation of small pores. After reconstruction of the UHT, the small pores less than 3 nm disappeared and the pore size distribution shifted to a maximum at 50 nm, presumably by the re-formation of the layers with an overall morphology similar to that of the parent UHT. Interestingly, the surface area of the reconstructed UHT was 3–4 times greater than that of the parent UHT sample. The as-prepared CHT sample started with a high BET surface area of 71 $m^2\ g^{-1}$, probably because the platelet size was much smaller than that of UHT. Moreover, the CHT sample had a maximum in the pore size distribution of 20 nm (Fig. 4) with a pore volume of 0.36 $cm^3\ g^{-1}$ (Table 1). The BET surface area and pore volume of the CHT sample increased to 252 $m^2\ g^{-1}$ and 0.62 $cm^3\ g^{-1}$, respectively, upon thermal decomposition. The pore size distribution had a maximum at 20 nm, which was similar to that of CHT, and was significantly greater than that of its precursor, in agreement with the reported results by Abello et al. [19]. Similar to UHT-d, some small pores less than 3 nm were also formed on the CHT-d sample. Upon reconstruction of the CHT-d sample, the small pores less than 3 nm disappeared on both CHT-d-rg and CHT-d-rl. The CHT-d-rg sample displayed a similar pore

size distribution to CHT, whereas CHT-d-rl displayed a pore size distribution with a maximum at about 50 nm, similar to UHT-d-rl.

3.6. Infrared spectroscopy

Infrared spectroscopy has been used extensively to characterize hydrotalcite and related materials [6,19,39–42]. The DRIFTS spectra of the fresh and activated hydrotalcite samples are displayed in Fig. 5. The spectra of hydrotalcite are consistent with those reported previously, except for minor shifts in peak positions. The spectra of both fresh CHT and UHT were similar, which is consistent with the similarity of their composition. The broad band at ~3420 cm^{-1} is attributed to the stretch of the H-bonded hydroxyl groups of the brucite-like layers and the broad shoulder at ~3020 cm^{-1} results from the H-bonding between the interlayer water and carbonate anion in the interlayer region. The sharp feature at 1360 cm^{-1} is assigned to the asymmetric stretching of carbonate anion (υ_3 mode), whereas the shoulder at ~1390 cm^{-1} could be due to the split υ_3 vibration of carbonate [19,40]. The out of plane (υ_2) and in plane (υ_4) bending of carbonate were also detected at ~870 and ~680 cm^{-1}, respectively [39]. The symmetric stretching of carbonate (υ_1) at 1064 cm^{-1} was not observed since it is infrared inactive [41]. The bending of water, typically observed at ~1640 cm^{-1} has shifted to 1570 cm^{-1} for UHT and 1540 cm^{-1} for CHT. The bands appearing at ~790 cm^{-1} can be ascribed to the translational mode of hydroxyl groups influenced by the aluminum, which has deformation modes at 935 cm^{-1} [42]. Upon decomposition of UHT and CHT, the intensity of the broad band between 2500 and 3700 cm^{-1} decreased significantly due to interlayer water removal and dehydroxylation of brucite-like layers. The υ_3 vibration of carbonate split into two bands at about 1405 and 1495 cm^{-1} due to the stronger interaction between CO_3^{2-} and Mg^{2+} after decomposition. Apparently, the decomposition at 723 K for 8 h did not completely decompose the hydrotalcite; however, reconstruction is known to be problematic if hydrotalcite is decomposed at too high of a temperature [34]. Both the liquid-phase and gas-phase reconstructions led to successful re-formation of the layered structures. The broad hydroxyl band stretch from 2500 to 3700 cm^{-1} reappeared and the bending mode of water shifted to 1600 cm^{-1}. The band at 1365 cm^{-1} that corresponded to the carbonate υ_3 asymmetric stretching mode was still present, presumably due to the incomplete decomposition of hydrotalcite or CO_2 contamination during DRIFTS sample preparation [19].

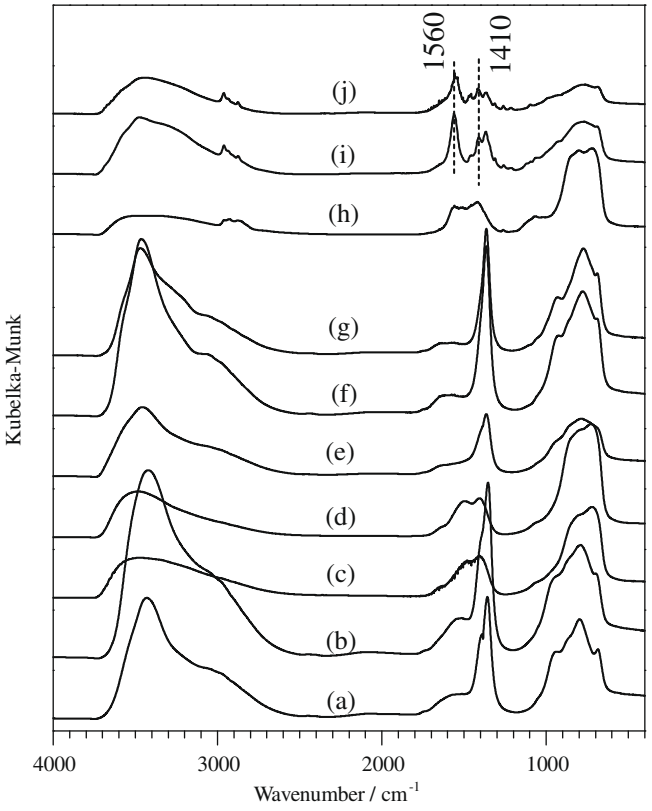

Fig. 5. Diffuse reflectance infrared Fourier transformed spectra (DRIFTS) of (a) CHT; (b) UHT; (c) CHT-d; (d) UHT-d; (e) CHT-d-rg; (f) CHT-d-rl; (g) UHT-d-rl; (h) recycled CHT-d after 2 runs; (i) recycled CHT-d-rl after 2 runs (purified tributyrin and anhydrous methanol were used as reactants); and (j) butyric acid-treated CHT-d-rl.

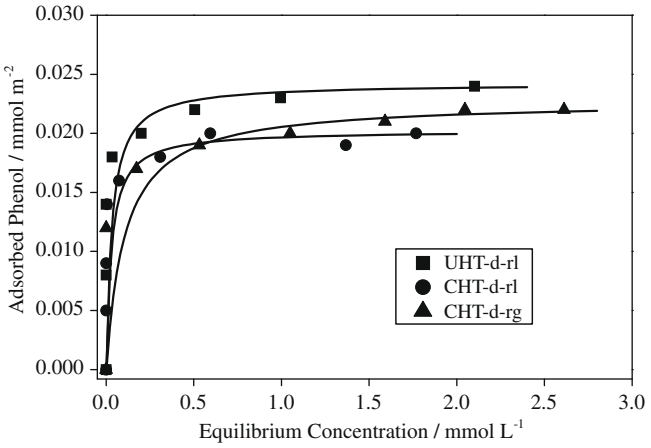

Fig. 6. Phenol adsorption isotherm of reconstructed hydrotalcite samples. Solid curves represent the fits to the Langmuir adsorption isotherm equation.

3.7. Phenol adsorption

Phenol adsorption has been reported to be an effective method to measure the surface base site density of porous solids [22,43–45]. One of the advantages of phenol adsorption on the solid catalysts is that no pretreatment, such as heating or evacuation, is necessary prior to the adsorption experiment. This is especially important for the case of reconstructed hydrotalcite because we reported previously that heat treatment can significantly alter the nature and the activity of the reconstructed hydrotalcite catalyst [15]. The phenol adsorption isotherms of the reconstructed hydrotalcite samples are presented in Fig. 6. All three isotherms were of the Langmuir type, indicating chemisorption of phenol on the catalyst samples [44]. The fitted Langmuir isotherms are presented as solid curves in Fig. 6 and the densities of the base sites of the reconstructed hydrotalcite samples as represented by phenol monolayer coverage, X_m, are listed in Table 1. It can be seen that the densities of the base sites of all three reconstructed hydrotalcite samples are similar in the range of 0.020–0.024 mmol m^{-2}, which are about 20–30% of the total anticipated base sites based on the Al content. Since no expansion of the interlayer distance was observed by XRD after phenol adsorption, the phenol is assumed to adsorb on the surface accessible base sites only. The similarity of the base site densities among the samples contrasts their significantly different textural properties as observed by SEM, N_2 adsorption, and XRD.

3.8. Catalytic performance

3.8.1. Exclusion of diffusion limitation

The initial rate of tributyrin transesterification with methanol over CHT-d-rl did not vary with stirring speed over the range of 600–1000 rpm, suggesting that the reaction was not limited by

external mass transfer to the catalyst particles. The Weisz modulus [46], $\Phi = \frac{(r_T \rho_s)_{obs} R^2}{D_{eff}[T]}$, where r_T is the reaction rate of tributyrin (1.2×10^{-5}, 1.3×10^{-5}, and 1.8×10^{-5} mol s^{-1} g^{-1} for CHT-d-rl, UHT-d-rl, and CHT-d-rg, respectively), ρ_s is the catalyst particle density (2 g cm^{-3}), R is the catalyst particle radius (0.038 mm), $D_{eff} = (\varepsilon/\tau)D$ is the effective diffusion coefficient (ε and τ are void fraction and tortuosity factor of catalyst, assumed to be 0.5 and 3, respectively; D is diffusion coefficient estimated to be 1.6×10^{-5} cm^2 s^{-1} by using Wilke–Chang equation [47]), and [T] is the tributyrin concentration (0.7 mol L^{-1}), was used to evaluate the effect of internal diffusion. The Weisz modulus Φ was estimated to be 0.18, 0.20, and 0.28 for CHT-d-rl, UHT-d-rl, and CHT-d-rg, respectively. Since the effectiveness factor was greater than 0.95 for all the reconstructed samples, the effect of internal mass transfer on the observed rates was neglected.

3.8.2. Effect of activation

Typical reaction profiles are displayed in Fig. 7 and fitted reaction rate constants and deactivation parameters are summarized in Table 2. The turnover frequencies (TOFs) of the reconstructed hydrotalcite catalysts were based on base site density determined from the uptake of phenol on the reconstructed hydrotalcite catalysts. Since the layer-to-layer distance of the reconstructed hydrotalcite is about 3 Å [48], the Brønsted base sites located between two adjacent layers are not accessible to large molecules such as tributyrin. The solid curves in Fig. 7 represent typical results from the fitting procedure. The decomposed hydrotalcite catalysts (CHT-d and UHT-d) are mixed oxides that expose Lewis base sites and they exhibit moderate activity for transesterification as shown in runs 1 and 2 in Table 2. However, CHT-d sample was about four times more active than UHT-d sample on a surface area basis. The activity difference between CHT-d and UHT-d could be ascribed to a different basic oxide ion population on the catalyst surface. It is known that the synthesis method can have a strong influence on the basic properties of the mixed oxides derived from hydrotalcite [5,35,38]. Climent et al. reported that the basic character of the Lewis sites on decomposed hydrotalcite depends on the coordination environment around the exposed surface oxygen

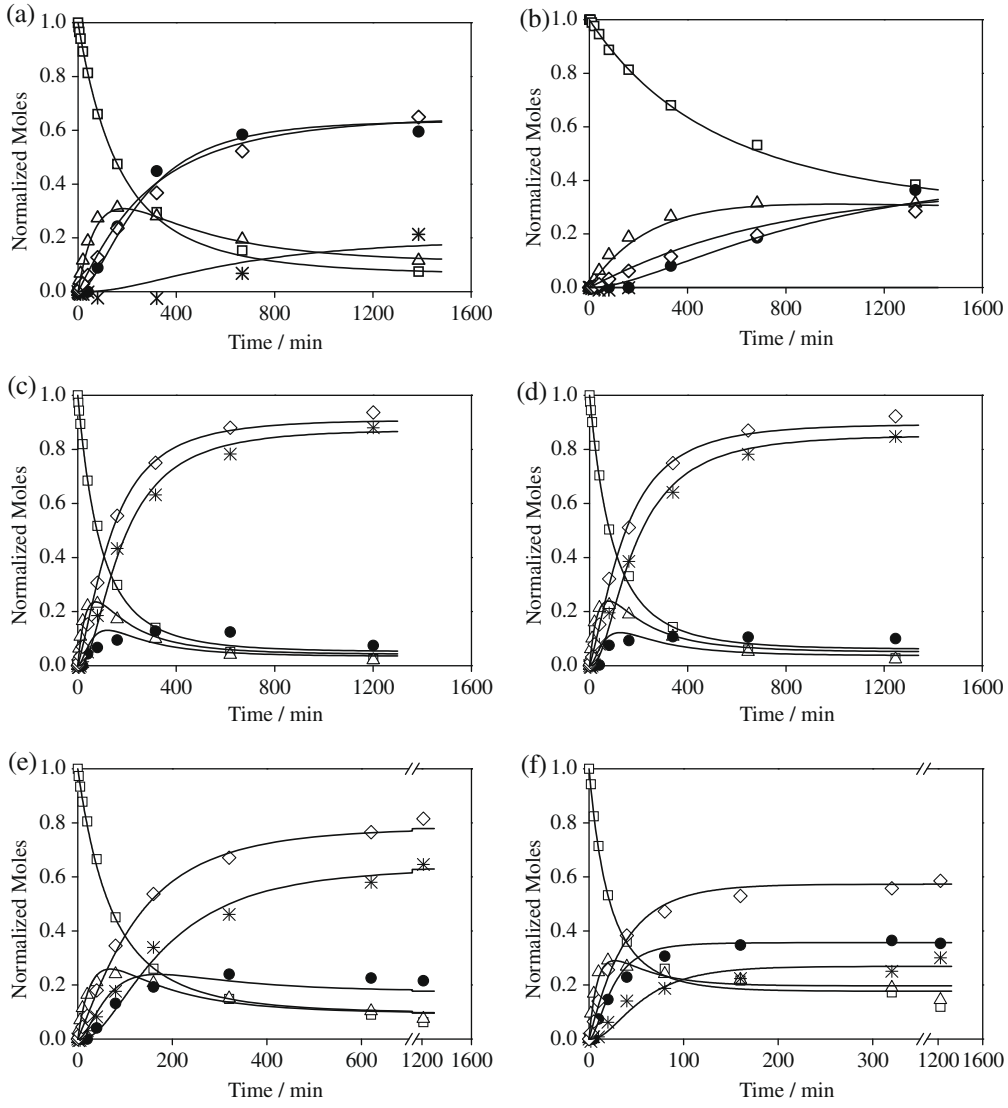

Fig. 7. Reaction profiles of transesterification of tributyrin with methanol catalyzed by activated 1 g of hydrotalcite samples: (a) CHT-d, (b) UHT-d, (c) CHT-d-rl, (d) UHT-d-rl, (e) CHT-d-rg with methanol wash, and (f) CHT-d-rg without methanol wash. Reaction conditions: methanol 68.25 g, tributyrin 21.9 g, and 333 K; The normalized moles for T, D, Mo, G, and MB are defined as $y_i = [i]/[T]_0$, where i = T, D, Mo, or G, and $y_{MB} = [MB]/[T]_0/3$, where [i] is the concentration of component i (mol L^{-1}) and $[T]_0$ is the initial concentration of tributyrin. (◇) methyl butyrate, (□) tributyrin, (Δ) dibutyrin, (●) monobutyrin, (*) glycerol (calculated by the mass balance between methyl butyrate, dibutyrin, monobutyrin, and glycerol, $y_G = (3y_{MB} - y_D - 2y_{Mo})/3$). The solid curves represent the calculated profiles.

Table 2
Comparison of decomposed hydrotalcites and reconstructed hydrotalcites as catalysts for the transesterification of tributyrin with methanol.

Run No.	Sample	k_1[a] ($\times 10^6$)	k_2[a] ($\times 10^6$)	k_3[a] ($\times 10^6$)	α[b]	TOF[c] ($\times 10^2$)	Conversion of tributyrin[d] (%)	Yield of methyl butyrate[d] (%)
1	CHT-d	1.9 ± 0.1	2.7 ± 0.3	0.35 ± 0.07	$(2.0 \pm 0.3) \times 10^{-3}$	–	90.3	69.0
2	UHT-d	0.49 ± 0.04	0.67 ± 0.1	–	$(1.1 \pm 0.2) \times 10^{-3}$	–	55.1	26.7
3	CHT-d-rl[e]	8.3 ± 0.5	18.3 ± 2.3	29.9 ± 5.9	$(3.4 \pm 0.4) \times 10^{-3}$	0.94	97.9	93.7
4	UHT-d-rl[e]	11.4 ± 0.7	24.5 ± 3.1	44.1 ± 9.4	$(3.5 \pm 0.4) \times 10^{-3}$	1.08	97.1	91.8
5a	CHT-d-rg[e]	16.3 ± 1.1	30.8 ± 3.9	25.6 ± 3.6	$(5.3 \pm 0.5) \times 10^{-3}$	1.64	94.5	81.4
5b	CHT-d-rg[f]	51.6 ± 3.5	80.3 ± 8.1	39.4 ± 4.6	$(2.3 \pm 0.2) \times 10^{-2}$	5.19	82.3	57.4
	$NaOCH_3$[g]	–	–	–	–	146[h]	~100[i]	>99[i]

[a] Reaction rate constant for activated hydrotalcite catalysts with 95% confidence interval (L mol^{-1} m^{-2} min^{-1}).
[b] Deactivation parameter with 95% confidence interval (min^{-1}).
[c] Turnover frequency (s^{-1}) was normalized to the number of base sites as determined from phenol adsorption.
[d] After 20 h reaction.
[e] Sample with methanol washing.
[f] Sample without methanol washing.
[g] Thousand microlitre of 0.0314 M sodium methoxide/methanol solution was used as catalyst. Purified tributyrin and anhydrous methanol were used as reactants.
[h] Turnover frequency was normalized to the moles of sodium methoxide.
[i] After 6 h reaction.

anions, with the strongest base sites being located on corners [35]. Therefore, a hydrotalcite with a smaller crystal size would likely form a greater concentration of strong Lewis base sites after decomposition. Chizallet et al. [49] and Bailly et al. [50] also observed that the MgO catalysts prepared by different routes have a different basic oxide ion population, as revealed by photoluminescence and catalytic activity for the conversion of 2-methylbut-3-yn-2-ol. Alternatively, the difference in activities between CHT-d and UHT-d could be related to textural properties of the samples. Fig. 4 shows that CHT-d has well-developed mesoporosity whereas UHT-d exhibits much smaller pore sizes which could restrict access of the reactants to the active sites. All the reconstructed hydrotalcite samples (runs 3–5 in Table 2) had a higher reaction rate constant k_1 than the decomposed ones (runs 1 and 2 in Table 2). This is consistent with the previously reported results [12,15,17,51–53].

3.8.3. Effect of textural properties of reconstructed hydrotalcite

The hydrothermally reconstructed hydrotalcite catalysts prepared from coprecipitation and urea hydrolysis, CHT-d-rl and UHT-d-rl, exhibit similar catalytic activity for transesterification reaction as shown in runs 3 and 4 in Table 2 and Fig. 7c and d. This result contrasts those of Lei et al. [22] and Greenwell et al. [21] who observed that a reconstructed hydrotalcite prepared by urea hydrolysis was more active than a reconstructed sample prepared by coprecipitation in a base-catalyzed aldol condensation reaction. Lei et al. [22] proposed that the adjacent hydroxyl groups on reconstructed hydrotalcite from urea hydrolysis are more ordered than those on reconstructed hydrotalcite from coprecipitation, which acted as acid–base pairs to efficiently catalyze the acetone self-condensation. However, the effect of the charge compensating hydroxyl anions, the Brønsted base sites, was not emphasized in that work. On the contrary, other studies have ruled out the catalytic role of the structural hydroxyl groups by comparing the very low catalytic activity of $Mg(OH)_2$ to that of highly active reconstructed hydrotalcite [12,15]. Therefore, the number and the location of the accessible Brønsted base sites (interlayer hydroxyl ions) should play more important roles for catalytic reaction, realizing that the Brønsted base sites of reconstructed materials derived from different reconstruction methods are similar in nature as concluded from the initial heat of CO_2 adsorption and the DRIFTS of adsorbed $CDCl_3$ [12].

The reaction profiles for transesterification over the methanol-washed reconstructed hydrotalcites are displayed in Fig. 7c–e. The reconstructed hydrotalcite samples, CHT-d-rl, UHT-d-rl, and CHT-d-rg exhibit significantly different textural properties as shown in Figs. 1 and 4. The UHT-d-rl sample has a larger platelet size of about 1.5–2.0 μm than that of CHT-d-rl with platelet size of about 150–250 nm, whereas they reveal a similar crystallite size determined by XRD along the normal directions of (0 0 *l*) and (1 1 0) as shown in Table 1. In contrast, the CHT-d-rg sample has a much smaller platelet size as well as a much smaller crystallite size than those of the CHT-d-rl and UHT-d-rl samples. Therefore, the CHT-d-rg sample was anticipated to exhibit much higher catalytic activity than CHT-d-rl and UHT-d-rl since the smaller crystallite size and smaller platelet size would likely expose more crystal edges and/or defects. The Brønsted base sites located near crystal edges and/or defects are considered to be more accessible for catalytic reactions [11,12,16,19]. However, a comparison of the rate constants in Table 2 for run 5a to those of runs 3 and 4 suggests a very modest influence of platelet and crystallite size on the transesterification rate, which contrasts the previous findings for aldol condensation [11,18,19] and styrene epoxidation [16]. Roeffaers et al. observed that the transesterification of 5-carboxyfluorescein with 1-butanol over [Li^+–Al^{3+}] layered double hydroxide catalyst occurs on the basal planes of the outer crystal surface without an appreciable preference for the crystal edges, whereas the hydrolysis reaction was favored on the crystal edges [20].

3.8.4. Effect of trace water

It is important to note that the activity of CHT-d-rg (Fig. 7e and Table 2) was significantly affected by the post-reconstruction washing with methanol. A sample of the same material used as a catalyst prior to washing with methanol, listed as 5b in Table 2 and shown in Fig. 7f had a rate constant k_1 of $(51.6 \pm 3.5) \times 10^{-6}$ L mol^{-1} m^{-2} min^{-1}, and a deactivation parameter α of $(2.3 \pm 0.2) \times 10^{-2}$ min^{-1}. Thus, the turnover frequency of the catalyst prior to methanol washing was 5.2×10^{-2} s^{-1}, which is more than triple the value found for the methanol-washed sample (run 5a, Table 2). Moreover, the deactivation parameter of the unwashed sample was nearly 5 times greater than that of the methanol-washed sample. Thus, we hypothesized the presence of trace water on the catalyst (either added intentionally or remaining on the catalyst from the reconstruction procedure) can impact the activity and stability of the layered double hydroxides for transesterification.

To further study the deactivation behavior of reconstruction hydrotalcite samples and the influence of water, purified tributyrin was used to exclude the possibility of deactivation due to trace amounts of carboxylic acid in the tributyrin reagent [54]. Hydrolysis of tributyrin was not observed during the purification process. Anhydrous methanol was also used as a reagent in some cases to exclude the unintentional addition of trace water. As a control test, purified tributyrin and anhydrous methanol were used as reactants

Table 3
Transesterification of tributyrin with methanol over reconstructed hydrotalcite CHT-d-rl.

Run No.	Reaction conditions	k_1[a] ($\times 10^6$)	k_2[a] ($\times 10^6$)	k_3[a] ($\times 10^6$)	α[b]	TOF[c] ($\times 10^2$)	Conversion of tributyrin[d] (%)	Yield of methyl butyrate[d] (%)
6	Purified tributyrin	8.3 ± 0.4	20.7 ± 2.1	45.5 ± 9.5	$(3.6 \pm 0.3) \times 10^{-3}$	0.93	96.8	91.7
7	Purified tributyrin, anhydrous methanol	5.7 ± 0.3	11.7 ± 1.2	18.5 ± 2.9	$(1.6 \pm 0.2) \times 10^{-3}$	0.64	98.7	97.6
8	Purified tributyrin, 100 μL of H_2O added	17.1 ± 1.3	44.9 ± 5.3	113 ± 24	$(1.8 \times 0.2) \times 10^{-2}$	1.93	74.1	55.9
9	Recycled after Run 6, washed with 200 ml of methanol	0.74 ± 0.05	1.2 ± 0.2	–	–	–	38.9	16.7
10	Recycled after Run 7, washed with 200 ml of methanol	3.5 ± 0.3	11.7 ± 1.7	–	–	–	87.7	76.5
11	Recycled after Run 8, washed with 200 ml of methanol	0.28 ± 0.04	–	–	–	–	17.2	6.3

[a] Reaction rate constant with 95% confidence interval (L mol^{-1} m^{-2} min^{-1}).
[b] Deactivation parameter with 95% confidence interval (min^{-1}).
[c] Turnover frequency (s^{-1}) was normalized to the number of base sites as determined from phenol adsorption.
[d] After 20 h reaction.

in the presence of 1000 μL of 0.0314 M sodium methoxide/methanol solution (prepared by diluting 0.5 M sodium methoxide/methanol solution (Aldrich) into anhydrous methanol) as a homogeneous catalyst. Fitting of the reaction profile indicated negligible catalyst deactivation, i.e. the deactivation constant was found to be zero. The turnover frequency of the sodium methoxide-catalyzed transesterification was estimated to be 1.46 s^{-1} as shown in Table 2.

From runs 6 to 11 in Table 3, CHT-d-rl was used as a catalyst and purified tributyrin was used as the reactant to test the influence of water on the reaction profile. The effect of trace water to the catalytic activity and stability of CHT-d-rl for the conversion of tributyrin can be clearly observed in Fig. 8. Runs 6 and 7 compare the effect of using anhydrous methanol to standard reagent grade methanol with a nominal water content of 0.04%. Although the run with anhydrous methanol had a lower rate constant k_1, it also had a lower deactivation parameter as shown in Table 3. Moreover, the yield of methyl butyrate in run 7 reached the highest value of 97.6% after 20 h. To further confirm that a small amount of water can not only significantly enhance the initial catalytic activity of the reconstructed hydrotalcite but also cause severe catalyst deactivation, run 8 was performed by purposely adding 100 μL of water to the reactants. The reaction rate constant k_1 of run 8 was about threefold higher than that of run 7, while also increasing the deactivation parameter α. However, the tributyrin conversion and methyl butyrate yield of run 8 only reached 74.1% and 55.9%, respectively, after 20 h of reaction as shown in Table 3 and Fig. 8. Runs 9, 10, and 11 present results from recycling the used catalysts from runs 6, 7, and 8 after centrifugation and washing with 200 ml of methanol. The system with the least amount of water in it (runs 7 and 10) showed the greatest activity upon recycle, obtaining 61% of the initial activity. The catalyst recycled from run 8 with the added water retained less than 2% of its initial catalytic activity (run 11) as shown in Table 3.

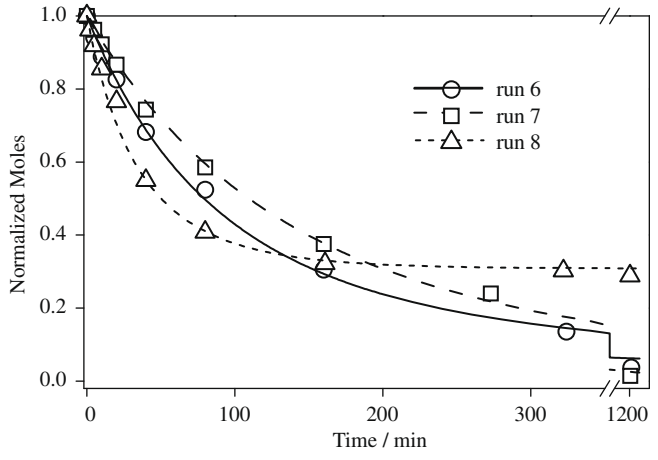

Fig. 8. Tributyrin reaction profiles of the reaction runs 6–8 illustrating the role of trace water on reactivity and stability of CHT-d-rl. Curves represent the fitted profiles.

3.8.5. Deactivation mechanism of reconstructed hydrotalcite catalysts

The deactivation of the reconstructed hydrotalcite can be ascribed to the hydrolysis of the ester molecules over the catalyst sample. The catalysts after two reaction runs were separated and analyzed by XRD and DRIFTS. The XRD patterns of the used reconstructed hydrotalcite samples revealed significant structural modification while the used decomposed hydrotalcite did not. Representative XRD patterns of used decomposed hydrotalcite and used reconstructed hydrotalcite are shown in Fig. 2h and i. The XRD pattern of decomposed hydrotalcite is identical to the pattern before reaction, which agrees with a previous study involving aldol condensation [23]. For the case of the reconstructed sample, the intensities of the original (0 0 3), (0 0 6), and (1 1 3) reflections decreased substantially and additional reflections at 6.2° and 18.3° were now observed after reaction. We suspected that butyric anions intercalated into the interlayer galleries thus expanding the layers. Therefore, a reconstructed sample was purposefully exposed to butyric acid and evaluated by XRD. Fig. 2j shows an XRD pattern that corresponds to the acid-treated sample, which confirms the idea that butyric anion is present in the interlayer gallery. Thus, the new XRD peak at 6.2° is assigned to the new (0 0 3) reflection of layered double hydroxide intercalated with butyric anion with a corresponding interlayer distance of 14.3 Å. The alkyl chains of butyric anions are assumed to form a bilayer arrangement in the interlayer space [55]. If the intercalated butyric anions have all-trans conformation in the interlayer region, the corresponding slant angle (the angle from the carboxylate chain to the normal of brucite-like layer) of the butyric anion carbon chain is about 55° according to the correlation between interlayer distance and the number of carbons in the carboxylate anion obtained by Nhlapo et al. [56]. The carboxylate anion can also be observed in the DRIFTS spectra of the recycled samples as shown in Fig. 5i and j. The new bands at 1560 and 1410 cm^{-1} are the asymmetric and symmetric stretches of carboxylate anions [56–58]. On the other hand, there were some organic compounds adsorbed on the mixed oxides after two runs as revealed by the C–H stretching

band around 2800–3000 cm^{-1} in Fig. 5h. Since bands at 1710 cm^{-1} associated with C=O of ester molecule and at 1410 cm^{-1} (symmetric stretching) and 1560 cm^{-1} (asymmetric stretching) of carboxylate were not detected, the likely adsorbed organics were methanol and/or glycerol.

The proposed mechanism of transesterification on reconstructed hydrotalcite is depicted in Scheme 1. The catalysis likely occurs through a path that is similar to the homogeneous base-catalyzed transesterification [59]. The first step is thought to be the deprotonation of methanol by a Brønsted base site, forming methoxide anion. The methoxide then attacks the carbonyl group of triglyceride to form a tetrahedral intermediate. The third step involves electron pair migration to form a new ester and a new alkoxide. The last step is the protonation of the alkoxide to regenerate the Brønsted base. In this mechanism, water is not directly involved in the second and third steps. However, based on a density functional theory study of the transesterification by tert-butoxide MgAl anionic clay, the presence of water was found to facilitate the formation of the tetrahedral intermediate in the second step, to polarize the C–O bond of the tetrahedral intermediate, and enhance the abstraction of the alkoxy group in the third step [60]. Their conclusions are consistent with the rate enhancement observed in our work resulting from physisorbed water on the catalyst or water present in the reagents. Moreover, the involvement of interlayer water on the transesterification reaction cannot be excluded.

Based on the results from XRD and DRIFTS, the deactivation path is similar to the saponification reaction as shown in Scheme 1, where the Brønsted base directly attacks the carbonyl carbon in an ester molecule forming the tetrahedral intermediate. The electron pair migration in the second step leads to the formation of the butyric acid. The rapid proton transfer from the acid to the alkoxide leads to the deactivation of the reconstructed hydrotalcite catalyst. Although water is not directly involved in this simplified mechanism, apparently, physisorbed water and/or impurity water from reactant medium enhanced the hydrolysis reaction and subsequent deactivation of reconstructed hydrotalcite catalysts. Based on first-principles calculations of basic hydrolysis of carboxylic acid ester under aqueous conditions, the presence of water assists the formation of tetrahedral intermediate [61] and significantly drops the energy barrier for the decomposition of the tetrahedral intermediate [62,63]. Meanwhile, the interlayer water may be also partially responsible for the deactivation of reconstructed hydrotalcite catalysts.

The process of the interlayer expansion of the reconstructed hydrotalcite catalyst during the deactivation can be described in a 3-step sequence as illustrated in Scheme 2. In the first step, the hydroxyl anions of the catalyst, presumably located at the edges or defects [20], react to form the butyric anions. The butyric anions diffuse into the galleries between the brucite-like layers and expand the interlayer distance to 14.3 Å as observed by XRD.

4. Conclusions

Hydrotalcite samples with Mg/Al molar ratio of 2 were synthesized by coprecipitation and urea hydrolysis. Although both decomposed samples and reconstructed samples were active for tributyrin transesterification with methanol, the samples that were reconstructed were significantly more active than the decomposed mixed oxides on a surface area basis. The reconstructed hydrotalcites prepared by different precursors and different reconstruction methods had significantly different textural properties, such as platelet size, pore size distribution, and crystallite size. However, the surface base site densities as determined by phenol adsorption are similar and no significant difference in catalytic activity was

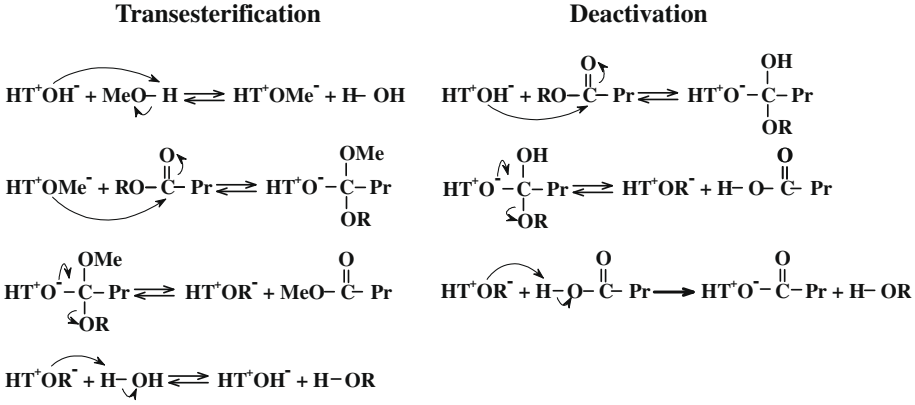

Scheme 1. Mechanism of reconstructed hydrotalcite-catalyzed transesterification reaction and deactivation. HT represents the hydrotalcite layer; Me represents methyl group, and Pr represents propyl group.

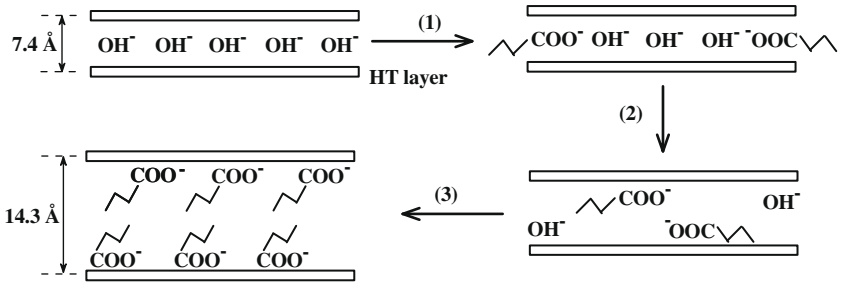

Scheme 2. Process of layer expansion during deactivation of reconstructed hydrotalcite. The intercalated butyric anions are assumed to form a bilayer arrangement in the interlayer spaces [55].

observed for the transesterification reaction. The presence of water (either physisorbed on the catalyst or present in the reactants) enhanced the rate of transesterification on reconstructed hydrotalcite catalysts. Unfortunately, water also accelerated the hydrolysis side reaction that deactivated the reconstructed hydrotalcite catalysts. The results from XRD and DRIFTS confirmed that deactivation of the reconstructed hydrotalcite samples was due to the replacement of the Brønsted base sites by the formed butyric anions through hydrolysis of esters.

Acknowledgments

This work was supported by the Chemical Sciences, Geosciences, and Biosciences Division, Office of Basic Energy Sciences, Office of Science, US Department of Energy, Grant No. DE-FG02-95ER14549.

References

[1] H. Hattori, Chem. Rev. 95 (1995) 537.
[2] B.F. Sels, D.E. De Vos, P.A. Jacobs, Catal. Rev. Sci. Eng. 43 (2001) 443.
[3] H. Hattori, Appl. Catal. A 222 (2001) 247.
[4] K. Tanabe, W.F. Holderich, Appl. Catal. A 181 (1999) 399.
[5] F. Cavani, F. Trifiro, A. Vaccari, Catal. Today 11 (1991) 173.
[6] J.I. Di Cosimo, V.K. Diez, M. Xu, E. Iglesia, C.R. Apesteguia, J. Catal. 178 (1998) 499.
[7] W.T. Reichle, J. Catal. 94 (1985) 547.
[8] S. Velu, C.S. Swamy, Appl. Catal. A 119 (1994) 241.
[9] A. Beres, I. Palinko, I. Kiricsi, J.B. Nagy, Y. Kiyozumi, F. Mizukami, Appl. Catal. A 182 (1999) 237.
[10] J. Roelofs, A.J. van Dillen, K.P. de Jong, Catal. Lett. 74 (2001) 91.
[11] J. Roelofs, D.J. Lensveld, A.J. van Dillen, K.P. de Jong, J. Catal. 203 (2001) 184.
[12] F. Winter, X. Xia, B.P.C. Hereijers, J.H. Bitter, A.J. van Dillen, M. Muhler, K.P. de Jong, J. Phys. Chem. B 110 (2006) 9211.
[13] B.M. Choudary, M.L. Kantam, C.R.V. Reddy, K.K. Rao, F. Figueras, J. Mol. Catal. A: Chem. 146 (1999) 279.
[14] D.G. Cantrell, L.J. Gillie, A.F. Lee, K. Wilson, Appl. Catal., A 287 (2005) 183.
[15] Y. Xi, R.J. Davis, J. Catal. 254 (2008) 190.
[16] R.J. Chimentao, S. Abello, F. Medina, J. Llorca, J.E. Sueiras, Y. Cesteros, P. Salagre, J. Catal. 252 (2007) 249.
[17] J. Roelofs, A.J. van Dillen, K.P. de Jong, Catal. Today 60 (2000) 297.
[18] F. Winter, V. Koot, A.J. van Dillen, J.W. Geus, K.P. de Jong, J. Catal. 236 (2005) 91.
[19] S. Abello, F. Medina, D. Tichit, J. Perez-Ramirez, J.C. Groen, J.E. Sueiras, P. Salagre, Y. Cesteros, Chem. Eur. J. 11 (2005) 728.
[20] M.B.J. Roeffaers, B.F. Sels, H. Uji-i, F.C. De Schryver, P.A. Jacobs, D.E. De Vos, J. Hofkens, Nature 439 (2006) 572.
[21] H.C. Greenwell, P.J. Holliman, W. Jones, B.V. Velasco, Catal. Today 114 (2006) 397.
[22] X.D. Lei, F. Zhang, L. Yang, X. Guo, Y. Tian, S. Fu, F. Li, D.G. Evans, X. Duan, AIChE J. 53 (2007) 932.
[23] S. Abello, D. Vijaya-Shanker, J. Perez-Ramirez, Appl. Catal., A 342 (2008) 119.
[24] Y. Liu, E. Lotero, J.G. Goodwin, C. Lu, J. Catal. 246 (2007) 428.
[25] D.E. Lopez, J.G. Goodwin, D.A. Bruce, E. Lotero, Appl. Catal., A 295 (2005) 97.
[26] U. Costantino, F. Marmottini, M. Nocchetti, R. Vivani, Eur. J. Inorg. Chem. (1998) 1439.
[27] W.T. Reichle, S.Y. Kang, D.S. Everhardt, J. Catal. 101 (1986) 352.
[28] M. Rajamathi, G.D. Nataraja, S. Ananthamurthy, P.V. Kamath, J. Mater. Chem. 10 (2000) 2754.
[29] G.S. Thomas, P.V. Kamath, J. Chem. Sci. 118 (2006) 127.
[30] A.V. Radha, P.V. Kamath, C. Shivakumara, Acta Crystallogr., Sect. B: Struct. Sci. 63 (2007) 243.
[31] A.V. Radha, P.V. Kamath, C. Shivakumara, J. Phys. Chem. B 111 (2007) 3411.
[32] M. Bellotto, B. Rebours, O. Clause, J. Lynch, D. Bazin, E. Elkaim, J. Phys. Chem. 100 (1996) 8527.
[33] M. Adachi-Pagano, C. Forano, J.P. Besse, J. Mater. Chem. 13 (2003) 1988.
[34] F. Rey, V. Fornes, J.M. Rojo, J. Chem. Soc. Faraday Trans. 88 (1992) 2233.
[35] M.J. Climent, A. Corma, S. Iborra, K. Epping, A. Velty, J. Catal. 225 (2004) 316.
[36] P. Benito, F.M. Labajos, V. Rives, Cryst. Growth Des. 6 (2006) 1961.
[37] G.M. Lombardo, G.C. Pappalardo, Chem. Mater. 20 (2008) 5585.
[38] D. Tichit, M.H. Lhouty, A. Guida, B.H. Chiche, F. Figueras, A. Auroux, D. Bartalini, E. Garrone, J. Catal. 151 (1995) 50.
[39] W.S. Yang, Y. Kim, P.K.T. Liu, M. Sahimi, T.T. Tsotsis, Chem. Eng. Sci. 57 (2002) 2945.
[40] S.K. Sharma, P.K. Kushwaha, V.K. Srivastava, S.D. Bhatt, R.V. Jasra, Ind. Eng. Chem. Res. 46 (2007) 4856.
[41] L. Hickey, J.T. Kloprogge, R.L. Frost, J. Mater. Sci. 35 (2000) 4347.
[42] F. Millange, R.I. Walton, D. O'Hare, J. Mater. Chem. 10 (2000) 1713.
[43] M.A. Aramendia, V. Borau, C. Jimenez, J.M. Marinas, F. Rodero, Colloids Surf. 12 (1984) 227.
[44] I. Rousselot, C. Taviot-Gueho, J.P. Besse, Int. J. Inorg. Mater. 1 (1999) 165.
[45] K. Parida, J. Das, J. Mol. Catal. A: Chem. 151 (2000) 185.
[46] P.B. Weisz, Adv. Catal. 13 (1962) 137.
[47] C.R. Wilke, P. Chang, AIChE J. 1 (1955) 264.
[48] J. Perez-Ramirez, S. Abello, N.M. van der Pers, Chem. -Eur. J. 13 (2007) 870.
[49] C. Chizallet, M.L. Bailly, G. Costentin, H. Lauron-Pernot, J.M. Krafft, P. Bazin, J. Saussey, M. Che, Catal. Today 116 (2006) 196.
[50] M.L. Bailly, C. Chizallet, G. Costentin, J.M. Krafft, H. Lauron-Pernot, M. Che, J. Catal. 235 (2005) 413.
[51] M.J. Climent, A. Corma, S. Iborra, A. Velty, Green Chem. 4 (2002) 474.
[52] M.J. Climent, A. Corma, S. Iborra, A. Velty, Catal. Lett. 79 (2002) 157.
[53] K.K. Rao, M. Gravelle, J.S. Valente, F. Figueras, J. Catal. 173 (1998) 115.
[54] W.L.F. Armarego, C.L.L. Chai, Purification of Laboratory Chemicals, fifth ed., Butterworth-Heinemann, 2003. p. 64.
[55] E. Kandare, J.M. Hossenlopp, J. Phys. Chem. B 109 (2005) 8469.
[56] N. Nhlapo, T. Motumi, E. Landman, S.M.C. Verryn, W.W. Focke, J. Mater. Sci. 43 (2008) 1033.
[57] C.R. Gordijo, V.R.L. Constantino, D.D. Silva, J. Solid State Chem. 180 (2007) 1967.
[58] C.A. Antonyraj, S. Kannan, Appl. Catal., A 338 (2008) 121.
[59] U. Schuchardt, R. Sercheli, R.M. Vargas, J. Braz. Chem. Soc. 9 (1998) 199.
[60] H.C. Greenwell, S. Stackhouse, P.V. Coveney, W. Jones, J. Phys. Chem. B 107 (2003) 3476.
[61] J.R. Pliego, J.M. Riveros, Chem. -Eur. J. 8 (2002) 1945.
[62] F. Haeffner, C.H. Hu, T. Brinck, T. Norin, J. Mol. Struct. -Theochem. 459 (1999) 85.
[63] C.G. Zhan, D.W. Landry, R.L. Ornstein, J. Am. Chem. Soc. 122 (2000) 2621.
[64] A.R. West, Solid State Chemistry and its Applications, John Wiley & Sons, 1984. p. 174.